The massive star binary fraction in young open clusters – III. IC 2944 and the Cen OB2 association

H. Sana,[1,2]★ G. James[3] and E. Gosset[4]†

[1]*Sterrenkundig Instituut Anton Pannekoek, Universiteit van Amsterdam, Science Park 904, 1098 XH Amsterdam, the Netherlands*
[2]*European Southern Observatory, Alonso de Cordova 1307, Casilla 19001, Santiago 19, Chile*
[3]*European Southern Observatory, Karl-Schwarzschild-Strasse 2, D-85748 Garching bei München, Germany*
[4]*Astrophysical Institute, Liège University, Bât. B5c, Allée du 6 Août 17, B-4000 Liège, Belgium*

ABSTRACT

Using an extended set of multi-epoch high-resolution high signal-to-noise ratio optical spectra, we readdress the multiplicity properties of the O-type stars in IC 2944 and in the Cen OB2 association. We present new evidence of binarity for five objects and we confirm the multiple nature of another two. We derive the first orbital solutions for HD 100099, HD 101436 and HD 101190 and we provide additional support for HD 101205 being a quadruple system. The minimal spectroscopic binary fraction in our sample is $f_{min} = 0.57$. Using numerical simulations, we show that the detection rate of our observational campaign is close to 90 per cent, leaving thus little room for undetected spectroscopic binary systems. The statistical properties of the O-star population in IC 2944 are similar, within the uncertainties, to the results obtained in the earlier papers in this series despite the fact that sample size effects limit the significance of the comparison. Using newly derived spectroscopic parallaxes, we reassess the distance to IC 2944 and obtained 2.3 ± 0.3 kpc, in agreement with previous studies. We also confirm that, as far as the O stars are concerned, the IC 2944 cluster is most likely a single entity.

Key words: binaries: close – binaries: spectroscopic – stars: early-type – open clusters and associations: individual: Cen OB2 – open clusters and associations: individual: IC 2944.

1 INTRODUCTION

Best known for its spectacular group of globules (Thackeray 1950; Reipurth et al. 1997; Reipurth, Raga & Heathcote 2003), IC 2944 is both an H II region and a rich stellar complex at the inner edge of the Carina spiral arm. Although the stellar aggregate formed by the bright OB stars in the vicinity of HD 101205 (O7 IIIn((f)); Walborn 1973) is located closer to the IC 2948 H II region, Collinder (1931) catalogued it as IC 2944. The same global group of stars was further listed as the Cen OB2 association by Alter et al. (1970). The whole complex is embedded in the large ionization region RCW 62, that includes the smaller IC 2944 and IC 2948 H II regions and extends over about 1 deg². Some authors (e.g. Kharchenko et al. 2005) also distinguished the separate stellar cluster IC 2948, which is formed by the few bright stars around HD 101413, at ∼12 arcmin south-east of HD 101205, and placed both entities at different distances. As a result, these stars have double entries in the stellar cluster data base WEBDA (Mermilliod 1992). In this paper,

we follow the earlier approach of Collinder (1931) and Ardeberg & Maurice (1977) and we use the IC 2944 denomination for the complete stellar aggregate at the core of RCW 62. The homogeneity of the region and its distance will be discussed later in this paper.

Thackeray & Wesselink (1965) performed the first extensive photometric and spectroscopic study of the cluster. They identified 14 early B- and nine O stars, and deduced a distance $d \approx 2.0 \pm 0.2$ kpc. Several authors subsequently questioned the physical reality of the cluster. Ardeberg & Maurice (1980) suggested that the stellar aggregate was rather formed by several distinct stellar groups, with distances ranging from 0.7 to 4 kpc. Perry & Landolt (1986) concluded that the apparent stellar concentration of IC 2944 resulted from the superposition of isolated early-type stars along the line of sight. Walborn (1987) reaffirmed, as far as the O-type stars are concerned, the physical reality of the cluster and showed that the spectroscopic parallax of the O-type stars was in excellent agreement with the earlier distance proposed by Thackeray & Wesselink (1965). Polarimetric observations by Vega, Orsatti & Marraco (1994) confirmed that some of the groups identified by Ardeberg & Maurice (1980) showed clear differences while others could not be separated from each other. The more recent study of Tovmassian et al. (1998), based on the ultraviolet (UV) space telescope *GLAZAR* on

★E-mail: h.sana@uva.nl
†F.R.S. – FNRS, Belgium.

board the Mir space station (Tovmassian et al. 1988), reassessed the situation. Studying 185 OBA stars in an area of 8 deg² towards Cen OB2, they confirmed that most of the O stars belong to IC 2944, at a distance of 2.2 ± 0.3 kpc. They further identified five other OB associations with distances ranging from 0.85 to 6.7 kpc (see their table 5).

As the third paper in our series, the present work readdress the spectral and multiplicity properties of the O-type star population in Cen OB2 and IC 2944. It is organized as follows. Section 2 summarizes the observing campaign and the data reduction. Section 3 discusses the individual objects. Section 4 evaluates the observational biases while Section 5 describes our results and Section 6 summarizes our work.

2 OBSERVATIONS AND DATA HANDLING

This paper is based on 166 high-resolution echelle spectra covering most of the optical spectrum of the targets. 97 of those spectra were obtained from 2004 to 2007 with the Fiber fed Extended Range Optical Spectrograph (FEROS) at the ESO 2.2-m telescope (La Silla, Chile) with a resolving power of 48 000. The other 69 spectra were taken from 2008 January to March using the UV–Visual Echelle Spectrograph (UVES) at the ESO Very Large Telescope (VLT)/Unit Telescope 2 (UT2; Paranal, Chile) operated in dichroic mode with the DIC2 437+760 set-up and a 0.8 arcsec entrance slit for both arms. The resulting resolving power is 50 000, thus almost identical to the FEROS one. The data reduction is similar to the one presented in Sana, Gosset & Evans (2009, hereafter Paper II) and the description will not be repeated here. The final, one-dimensional spectra were normalized to unity before merging the individual orders. The average signal-to-noise ratio (S/N) of the data set is well above 150.

Line profile fitting was performed with a semi-interactive code (FITLINE) developed by P. François at the Paris–Meudon Observatory and originally used in the context of chemical abundance determinations in globular cluster stars (James et al. 2004) or in extremely metal-poor halo stars (François et al. 2007). This code is based on a genetic algorithm approach (Charbonneau 1995) that mimics the way genetic mutations affect DNA, driving the evolution of species under given environmental constraints. In our case, lines are fitted by Gaussian profiles, each of them defined by four parameters: the central wavelength, the width and depth of the

line and the continuum value. Briefly, the algorithm proceeds as follows.

(i) An initial set of Gaussians is computed, giving random values to the four parameters. The quality of each fit is estimated by a χ^2 calculation.

(ii) A new 'generation' of Gaussians is then calculated from the 20 best fits after adding random modifications to the initial set of parameters ('mutations'). The new set replaces the old one, new fits are computed and the quality of these fits is estimated again by using a χ^2 evaluation.

(iii) The process is iterated typically several hundred times until convergence to the best Gaussian fits is attained.

(iv) A line-by-line interactive inspection of the fits is performed to remove bad fits, to correct the position of the continuum or to handle line blends in SB2 systems.

(v) The process is iterated again, and the profile parameters corresponding to the best fit are adopted.

The spectral lines considered in this process are listed in Table 1 together with the number of measurements available for each star. The equivalent width (EW) and the radial velocity (RV) of each line are computed based on the final fit, using the same rest wavelengths as adopted in other papers of this series. The rest wavelengths are further indicated in Table 2 that provides the journal of the observations and that lists, line-by-line, the RV measurements.

As in other papers in the series, we adopted the spectral classification criteria of Conti & Alschuler (1971), Conti (1973), Mathys (1988) and Mathys (1989) that rely on the EWs of given diagnostic lines. We used the usual notations: $\log W' = \log W(\lambda 4471) - \log W(\lambda 4542)$, $\log W'' = \log W(\lambda 4089) - \log W(\lambda 4144)$ and $\log W''' = \log W(\lambda 4388) + \log W(\lambda 4686)$, where the EWs are expressed in mÅ. The measurements and the corresponding spectral types are given in Table 3 and discussed in Section 3. The EWs of SB2 lines were measured at epochs of large separation only. Table 3 provides the actual observed values. For multiple systems, because of dilution by the companion continuum, the tabulated values of $\log W(\lambda 4686)$ and of $\log W'''$ should be regarded as lower limits.

In Sections 3.1 and 3.2, time series are searched for periodicities using the Fourier analysis of Heck, Manfroid & Mersch (1985) as amended by Gosset et al. (2001). Quoted uncertainties on the period values are adopted to correspond to one-tenth of the width of the associated peak in the periodograms. Whenever relevant, orbital

Table 1. Number of RV measurements obtained for each object with respect to the considered spectral lines. A '–' means that the corresponding line has not been measured.

Object	He I λ4026	Si IV λ4089	He I λ4144	He I λ4388	He I λ4471	Mg II λ4481	He II λ4542	He II λ4686	He I λ4922	He II λ5412	He I λ5876	He I λ7065
HD 100099	24	24	24	24	24	24	24	24	24	14	24	24
HD 101190	20	20	20	20	20	–	20	20	20	10	20	20
HD 101191	12	12	12	12	12	12	12	12	12	7	12	12
HD 101223	6	6	6	6	6	6	6	6	6	4	6	6
HD 101298	8	8	4	8	8	8	8	8	8	6	8	8
HD 101333	5	5	5	5	5	5	5	5	5	3	5	5
HD 101413	10	10	10	10	10	10	10	10	10	5	10	10
HD 101436	13	13	13	13	13	–	13	13	13	8	13	13
HD 101545A	7	7	7	7	7	7	7	7	7	5	7	7
HD 101545B	7	7	7	7	7	7	7	7	7	5	7	7
HD 308804	2	–	2	2	2	2	–	–	2	–	2	–
HD 308813	11	11	11	11	11	11	11	11	11	6	11	11
CPD −62°2198	6	6	6	6	6	5	6	6	6	4	6	6

Table 2. Journal of the spectroscopic observations of the O-type stars in IC 2944. First and second lines indicate the spectral line and the adopted rest wavelength (in Å). The first column gives the heliocentric Julian date at mid-exposure. The following columns provide, for each spectral line, the measured RVs (in km s^{-1}). References for the instrumental set-up can be found at the bottom of the table. The full table is available with the electronic version of the article (see Supporting Information).

HJD 2400000	He I λ4026 4026.072	Si IV λ4089 4088.863	He I λ4144 4143.759	He I λ4388 4387.928	He I λ4471 4471.512	Mg II λ4481 4481.228	He II λ4542 4541.590	He II λ4686 4685.682	He I λ4922 4921.929	He II λ5412 5411.520	He I λ5876 5875.620
HD 100099 prim											
53135.461[a]	−8.89	−16.29	−13.65	−12.42	−14.85	−14.58	−14.50	−10.13	−15.16	−14.97	−13.78
53509.559[a]	−74.59	−75.76	−74.01	−73.28	−75.24	−74.77	−73.25	−75.65	−75.47	−74.81	−75.03
53511.507[a]	−14.22	−20.77	−15.12	−14.20	−17.73	−20.62	−22.40	−15.43	−20.55	−21.60	−21.42
53512.476[a]	26.71	30.95	25.39	24.05	25.36	25.56	31.70	30.56	26.32	30.49	28.49
53860.551[a]	145.89	149.61	144.70	143.07	143.97	143.91	146.30	149.39	143.75	148.34	147.65
53860.704[a]	142.04	147.69	140.38	140.81	141.98	141.91	142.84	147.62	141.93	143.66	144.56
53861.510[a]	115.26	119.97	114.35	116.25	115.79	115.79	118.31	122.67	116.40	119.63	119.18
53861.688[a]	110.78	116.61	112.14	112.17	111.84	111.84	113.11	116.74	110.88	114.14	112.49
53862.485[a]	91.09	89.30	88.28	87.57	87.73	87.73	89.40	94.24	87.17	90.65	93.88
53862.681[a]	79.54	83.59	79.65	79.36	79.66	79.72	83.57	86.23	79.87	83.49	84.69
53863.489[a]	52.75	56.45	53.61	55.87	53.50	53.64	61.38	61.31	54.24	60.40	58.69
53863.730[a]	53.50	48.27	47.10	46.63	45.43	45.64	53.51	52.36	50.40	52.10	51.00
53864.501[a]	32.62	32.04	31.92	32.27	31.35	31.62	39.63	38.28	32.56	38.77	32.93
53864.727[a]	28.18	29.07	27.61	28.15	27.35	27.56	33.71	34.45	26.92	33.39	27.91
54493.820[b]	−7.53	−10.13	−2.45	−6.61	−10.22	−9.88	−9.94	−4.43	−9.98	–	−10.07
54513.845[b]	6.62	6.92	8.44	6.43	5.90	6.17	5.91	10.04	6.41	–	6.62
54514.883[b]	−1.89	−3.10	2.23	−1.64	−11.09	−5.39	−5.64	0.85	−1.67	–	−3.03
54515.814[b]	−8.62	−12.93	−12.48	−11.01	−12.50	−9.43	−8.93	−5.57	−12.33	–	−12.00
54521.779[b]	−76.11	−76.10	−75.95	−75.72	−75.58	−76.18	−75.98	−73.92	−75.82	–	−76.08
54532.799[b]	32.60	37.83	33.00	33.24	34.59	33.58	33.19	39.21	33.28	–	38.04
54537.857[b]	−10.93	−15.73	−11.57	−11.88	−18.57	−14.02	−19.16	−12.28	−16.41	–	−18.91
54539.811[b]	−39.02	−39.85	−38.62	−39.48	−45.75	−45.35	−45.88	−40.94	−44.74	–	−45.66
54540.817[b]	−50.82	−51.23	−51.31	−51.47	−55.34	−58.09	−55.58	−52.26	−52.34	–	−57.31
54544.539[b]	−76.68	−77.59	−76.09	−76.85	−78.97	−79.50	−75.40	−72.94	−78.83	–	−79.38

[a] ESO 2.2-m + FEROS.
[b] VLT + UVES.

Table 3. Diagnostic line ratios and corresponding spectral types for the studied O-type objects. Inapplicable criteria for specific cases are marked as n/a. We refer to text for discussion of the individual cases and to Table 9 for the finally adopted spectral types. Quoted error bars give the 1σ dispersions on the measurements.

Object	Component	$\log W'$	$\log W''$	$\log W(\lambda 4686)$	$\log W'''$	Spectral type
HD 100099	Prim	0.305 ± 0.066	0.292 ± 0.021	n/a	$>4.944 \pm 0.016$	O9 III/I
HD 100099	Sec	0.660 ± 0.067	-0.117 ± 0.054	n/a	$>4.361 \pm 0.062$	O9.7 V
HD 101190	Composite	-0.369 ± 0.023	n/a	2.737 ± 0.028	n/a	O5.5 V
HD 101191	Composite	0.131 ± 0.006	0.102 ± 0.032	2.864 ± 0.005	n/a	O8 V/III
HD 101223	n/a	0.148 ± 0.022	0.192 ± 0.054	2.777 ± 0.026	n/a	O8 V
HD 101298	n/a	-0.200 ± 0.035	0.423 ± 0.143	2.705 ± 0.037	n/a	O6–O6.5 V/III
HD 101333[a]	n/a	$0.315 - 0.666$	$0.118 - 0.144$	$5.25 - 5.69$	n/a	O9–O9.7 V/III
HD 101413	Prim	0.112 ± 0.017	-0.038 ± 0.021	$>2.793 \pm 0.013$	n/a	O8 V
HD 101436	Prim	-0.090 ± 0.050	0.302 ± 0.230	$>2.061 \pm 0.147$	n/a	O6.5–O7 V
HD 101436	Sec	-0.170 ± 0.107	n/a	$>2.761 \pm 0.062$	n/a	O5–O6 V
HD 101545	A	0.461 ± 0.041	0.282 ± 0.048	n/a	5.082 ± 0.067	O9.5 III
HD 101545	B	0.890 ± 0.179	0.234 ± 0.094	n/a	4.950 ± 0.060	O9.7 III/I
HD 308813	Prim	0.599 ± 0.025	0.015 ± 0.104	n/a	$>5.378 \pm 0.038$	O9.5 V
CPD $-62°2198$	n/a	0.663 ± 0.053	0.205 ± 0.083	n/a	5.110 ± 0.053	O9.7 III/I

[a]The nature of the adopted line profile is the dominant source of uncertainties, so that we rather quote here the range of values obtained by fitting either Lorentz or Gaussian profiles.

solutions are adjusted using the Liège orbital solution package (e.g. Sana, Gosset & Rauw 2006).

3 O-TYPE STARS IN IC 2944

3.1 SB2 systems

3.1.1 HD 101131

Close to the cluster core, HD 101131 is a known SB2 binary with O6.5 V((f)) and O8.5 V components. Gies et al. (2002) published a detailed analysis of the orbital properties. They derived a period P of 9.6 d and a slight eccentricity $e = 0.17 \pm 0.03$. Because HD 101131 is already well constrained, we did not reobserve it.

3.1.2 HD 101205

With a combined magnitude of $V = 6.45$, HD 101205 is a visual binary with a separation of 0.36 arcsec and $\Delta V = 0.3$ (Mason et al. 1998). It is also the brightest source in the cluster and a known eclipsing system with a period of 2.1 d (Balona 1992; Mayer, Lorenz & Drechsel 1992; Otero 2007). Additional photometry (Mayer et al. 2010) reveals however a more complicated light curve than expected for an eclipsing binary suggesting that the true nature of the system is not fully understood. We have acquired 20 FEROS spectra from 2004 to 2006 and 15 UVES spectra from 2008 January to March. Our data reveal a clear multiple signature in the He I lines and an SB1 motion and asymmetric profiles of the He II photospheric lines (Fig. 1). He II $\lambda 4686$ presents a mixed absorption and emission profile, with the main absorption component moving in phase with the primary and, possibly, a second fainter absorption component associated to the secondary. In the latter case, the third, overimposed emission component could be produced by wind–wind collision in such a short-period system, a situation similar to HD 152248 (Sana, Rauw & Gosset 2001).

The highest peak in the periodogram corresponds to a period of 2.8 d, a value significantly offset from the photometric period. Adopting this period, we have been able to fit the RVs using a circular orbital solution (as expected for such a short period system), yet the residuals are widely spread: 18 km s^{-1}. This is significantly
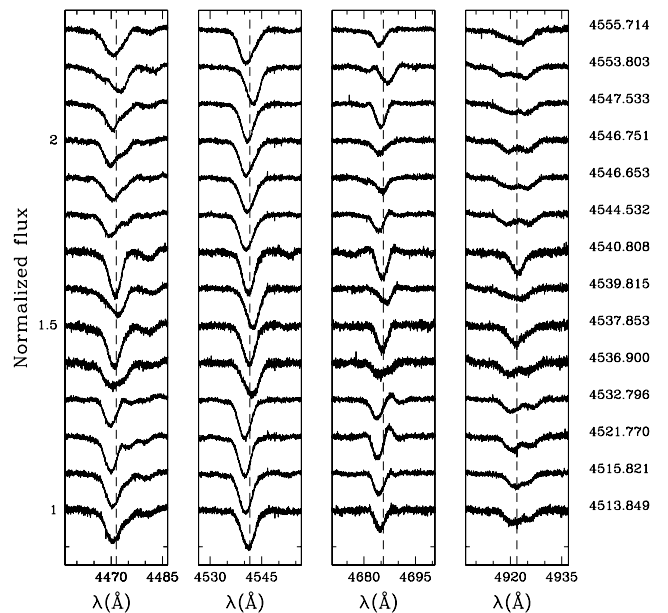

Figure 1. HD 101205: He I $\lambda 4471$, He II $\lambda\lambda 4542$, 4686 and He I $\lambda 4922$ line profiles at various epochs. The right-hand column gives the heliocentric Julian date (HJD) at mid-exposure in format HJD $- 2\,450\,000$. The vertical dashed lines indicate the rest wavelength.

larger than the expected RV accuracy (<5 km s^{-1}). This suggests either a systematic error in the measurements (e.g. the presence of a third spectroscopic component), or an additional variability signal. Naturally, the presence of the speckle companion implies that a third light spectral component must be present, and line blending would tend to reduce the measured velocity excursions. It is unclear whether it would however bias the periodicity of the signal. Finally, a multiperiodic analysis of the time series reveals, however, no extraperiodic signal on the time scales covered by our campaign, beside the 2.8 d period.

Our data set is unfortunately insufficient to solve the discrepancy between the photometric and spectroscopic periods. As noted by Mayer et al. (2010), the two visual components of HD 101205 might both be multiple systems. A dedicated monitoring is needed to

elucidate the nature of this object, which could be a new Trapezium system. The multiple nature of HD 101205 is, however, no longer in doubt.

3.1.3 HD 100099

At about $1°$ south-west of HD 101205, HD 100099 is associated to IC 2944 in the earlier works (e.g. Thackeray & Wesselink 1965) although Tovmassian et al. (1998) preferred to assign it to the Cen-Cru OB2.7 association. Based on the large angular separation of HD 100099 from the cluster centre, Baumgardt, Dettbarn & Wielen (2000) assigned to it a low membership probability but noted that its proper motion was still compatible with the kinematic properties of IC 2944.

HD 100099 was classified O9 III by Garrison, Hiltner & Schild (1977) and by Herbst (1975). We collected 24 spectra of this star that clearly revealed an SB2 system with two late O-type components (Fig. 2). Clear RV variations are seen from one night to the other, suggesting a relatively short period. Both He II and Si IV lines are definitely present in the secondary spectrum. Disentangling the secondary signature in the He II $\lambda4542$ region is more difficult because of the presence of N III $\lambda\lambda4534$–4545 in the primary spectrum that has a similar strength as the secondary He II $\lambda4542$ line. Reliable separation is achieved on a couple of spectra only. Our best estimate for the observed secondary He II $\lambda4542$ EW is 0.08 Å, and we used this value to derive the spectral type. Based on our measurements, the spectral type estimates are O9 and O9.7 for the primary and secondary stars, respectively, with the O8.5 and O9.5 spectral subtypes well within the respective uncertainties. The Si IV $\lambda4089$ over He I $\lambda4144$ line ratio, W'', indicates that the primary is likely a giant, with the supergiant class within the uncertainties, and that the secondary is likely a main-sequence star. Given the object's magnitude ($V = 8.09$), a supergiant primary would place the object at 4 to 5 kpc and a class III would place it at about 3 kpc. While HD 100099 is thus potentially a member of a different association (Tovmassian et al. 1998), its systemic velocity is compatible with the RVs of the other O stars in IC 2944.
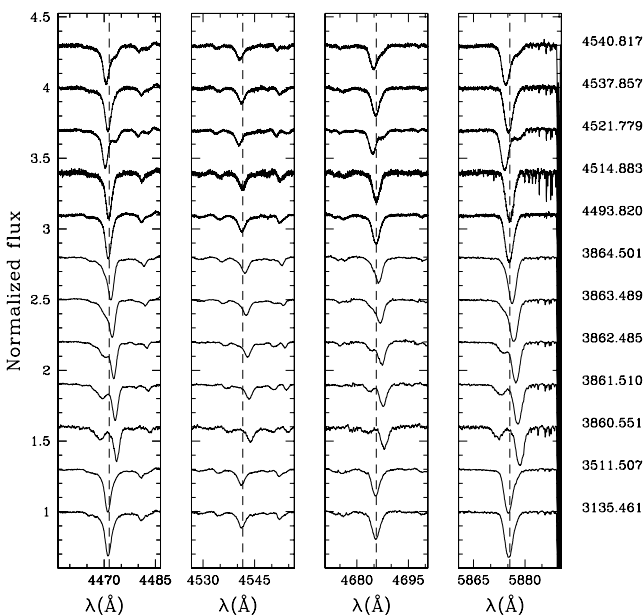
Figure 2. HD 100099: He I $\lambda4471$, He II $\lambda\lambda4542$, 4686 and He I $\lambda5876$ line profiles at various epochs.
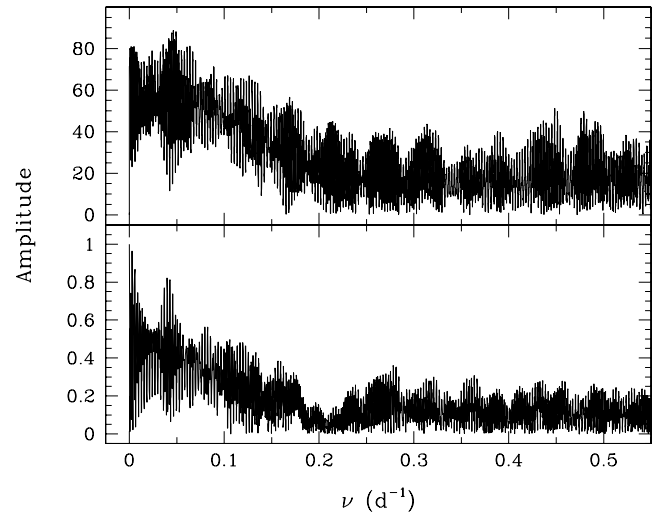
Figure 3. HD 100099: periodogram (upper panel) and spectral window (lower panel) computed from the He I $\lambda5876$ primary RV measurements.

Table 4. HD 100099: best-fitting orbital solution based on the He I $\lambda5876$ RV measurements. T (in HJD − 245 0000) is the time of periastron passage and is adopted as $\phi = 0.0$ in Fig. 4. Quoted uncertainties correspond to 1σ error bars.

Parameter	He I $\lambda5876$
P (d)	21.5585 ± 0.0330
e	0.517 ± 0.019
ω (°)	305.5 ± 0.9
T	2995.654 ± 0.078
γ_1 (km s^{-1})	16.5 ± 2.1
γ_2 (km s^{-1})	-6.0 ± 2.6
K_1 (km s^{-1})	138.4 ± 5.7
K_2 (km s^{-1})	174.8 ± 7.3
M_2/M_1	0.792 ± 0.013
$a_1 \sin i$ (R$_\odot$)	50.46 ± 2.20
$a_2 \sin i$ (R$_\odot$)	63.72 ± 2.78
$M_1 \sin^3 i$ (M$_\odot$)	24.0 ± 3.1
$M_2 \sin^3 i$ (M$_\odot$)	19.0 ± 2.4
rms (km s^{-1})	2.4

A detailed study of the orbital solution is beyond the scope of this paper. Here we limit ourselves to a preliminary analysis based on the He I $\lambda5876$ line. Our Fourier analysis indicates a most probable period close to 21.57 d, although we note that the corresponding peak in the periodogram is favoured by the sampling (Fig. 3). Best-fitting parameters and RV curves are displayed in Table 4 and in Fig. 4, respectively. While the fit is of good quality, our data do not sample the maximum separation epoch, leaving some uncertainties both on the RV curve semi-amplitudes K_1 and K_2 and on the eccentricity.

3.1.4 HD 101436

HD 101436 (O6.5 V; Walborn 1973) was flagged as a probable RV variable star by Thackeray & Wesselink (1965), with significant RV changes on a time-scale of a week. Two additional RV measurements by Humphreys (1973) and Conti, Leep & Lorre (1977) confirmed a ΔRV amplitude of ≈40 km s^{-1}. We obtained 13 additional spectra covering time scales from days to years that reveal,
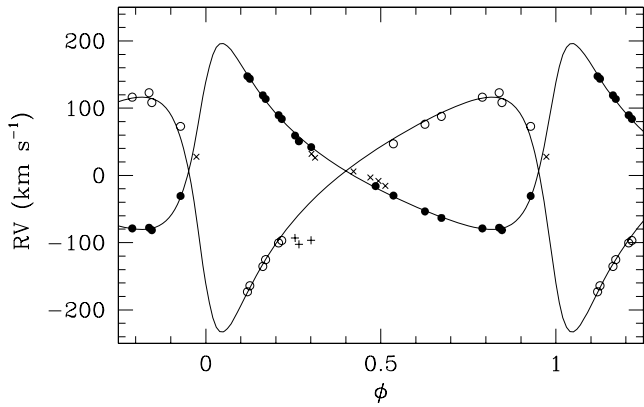
Figure 4. HD 100099: primary (filled symbols) and secondary (open symbols) RVs together with the best-fitting RV curves. The crosses indicate the data not taken into account in the fit because components could not be securely separated.
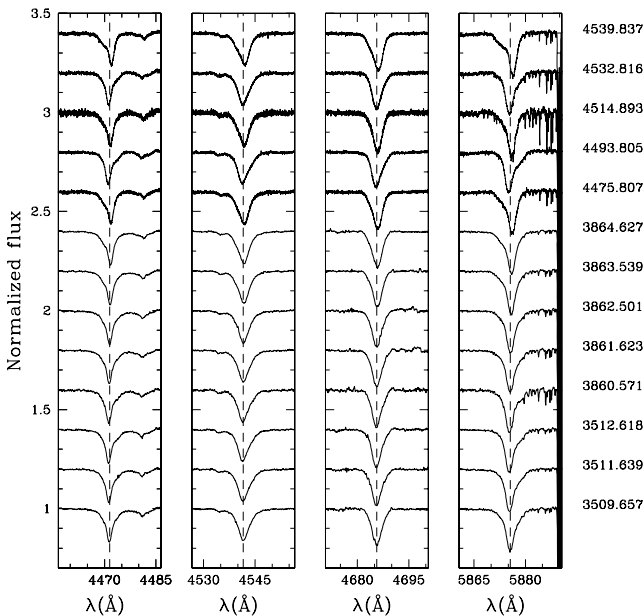

Figure 5. HD 101436: He I λ4471, He II λλ4542, 4686 and He I λ5876 line profiles at various epochs.

for the first time, a shallow secondary signature in the He I, He II and Si IV lines (Fig. 5). Fitted with a single Gaussian, the narrow (primary) component presents a clear and smooth increase over our 5-d campaign in 2006 May, rising by about $40 \, \text{km s}^{-1}$ from -20 to $+20 \, \text{km s}^{-1}$ approximately, although slightly depending on the line considered. Yet, RV measurements are hampered by a degeneracy in the determination of the line profiles. Two different hypotheses allow us to fit the data. Either the secondary contributes to the blended profile as a faint and narrow component or it contributes as a broad and shallow one. In both cases, however, the values of the Conti's criteria are left unaffected within the uncertainties, with the primary being an O7 star and the secondary, an O6.5 star with half subtype uncertainties on both measurements. Because the He I λ4144 line is very weak, the W'' criterion is unsuited and we relied on the $W(\lambda 4686)$ measurements to estimate the luminosity class. Depending on the adopted width for the secondary, the He II λ4686 line is dominated either by the primary or by the secondary star. The dominating component displays a strong absorption, typical of

dwarf stars. The other component shows then a measured value of $\log W(\lambda 4686) \approx 2.2$–2.3. Because the line is diluted by the companion continuum, this measurement provides only a lower limit on the true strength of the He II λ4686. It would correspond to a main-sequence star if the light ratio is 1:3 or more. Given the system magnitude, both stars are further expected to be main-sequence stars if located in IC 2944 and we adopt O7 V+O6.5 V as a tentative spectral classification.

To double-check the results of the RV genetic fitting algorithm, we also developed a global χ^2 minimization approach. We adjusted the profiles of the He I λλ4026, 4471, 5876 and of the He II λλ4200, 4542, 4686 lines simultaneously on all the 13 spectra using the following assumptions: (i) the profile of each line is formed by a blend of two Gaussian components representing the contribution of each star; (ii) the RV of each star is identical for all the lines at a given epoch and (iii) the amplitudes and full widths at half-maximum (FWHMs) of the Gaussians are identical for a given line and a given stellar component at all epochs. As a result, this approach definitely favours the second option of a narrow primary and a broad and shallow secondary.

As a final step, we replaced the Gaussian profiles by more realistic profiles. The latter were computed using FASTWIND (Puls et al. 2005) for a range of parameters typical of mid-O stars (Martins, Schaerer & Hillier 2005), then convolved with a rotational profile. Given the high spectral resolution of our data, we neglected the effect of the instrumental profile. Dilution by the companion continuum was included as a free parameter. To increase the realism of the approach, we further required that each line of a given component uses the same dilution factor and the same projected rotation rate. The best fit was obtained by using atmosphere models corresponding to the physical parameters of an O6 V primary with $v \sin i \approx 70 \, \text{km s}^{-1}$ and an O6.5 V secondary with $v \sin i \approx 200 \, \text{km s}^{-1}$.

While the overall line profiles are well reproduced in both approaches, the obtained RVs show systematic differences. On average, the RVs associated to the narrow component are $3 \, \text{km s}^{-1}$ smaller when using the FASTWIND profiles and the RVs of the broad component are $8 \, \text{km s}^{-1}$ larger. This has a significant impact on the respective amplitudes of the RV signal as well as on their ratio (Table 5).

Despite these uncertainties, the global χ^2 minimization improves the disentangling performances compared to the genetic algorithm described in Section 2, allowing us to constrain some of the orbital parameters. For both RV sets, a Fourier analysis indicates two most probable periods of 12.9 and 37.3 d, the second one presenting the highest peak in the periodograms. A preliminary orbital solution

Table 5. HD 101436: best-fitting orbital solution using RVs based on Gaussian profiles (column 2) and on atmosphere model profiles (column 3). T (in HJD − 245 0000) is the time of periastron passage. Quoted uncertainties correspond to 1σ error bars.

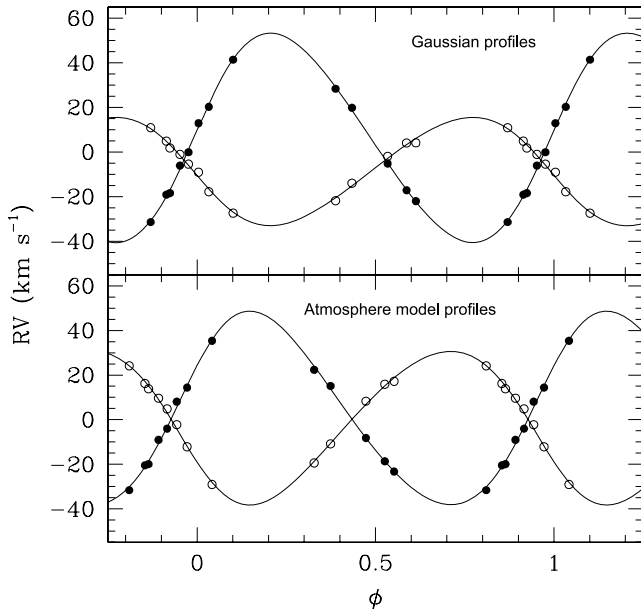| Parameter	Gaussian profiles	Atmosphere model profiles
P (d)	37.37 ± 0.14	37.37 ± 0.14
e	0.11 ± 0.01	0.11 ± 0.02
ω (°)	274 ± 12	296 ± 11
T	3190.77 ± 1.14	3193.04 ± 1.01
M_1/M_2	0.52 ± 0.02	0.79 ± 0.03
γ_1 (km s^{-1})	6.0 ± 0.8	3.2 ± 0.8
γ_2 (km s^{-1})	-8.7 ± 0.5	-2.2 ± 0.6
K_1 (km s^{-1})	46.9 ± 1.4	43.4 ± 1.1
K_2 (km s^{-1})	24.3 ± 0.7	34.4 ± 0.9
rms (km s^{-1})	1.3	1.4

Figure 6. HD 101436: primary (filled symbols) and secondary (open symbols) RVs together with the best-fitting RV curves of Table 5.

Figure 7. HD 101190: He I λ4471, He II $\lambda\lambda$4542, 4686 and He I λ5876 line profiles at various epochs.

analysis also favours the longer period. In both cases, slightly eccentric orbits provide a better fit compared to circular orbits. All in all, the orbital solutions built on both RV sets yield parameters in good agreement, except for the amplitude of the secondary RV curve and for the mass ratio. In particular, the RV measurements based on the more realistic FASTWIND profiles yield a mass ratio closer to unity, which is in better agreement with our spectral-type estimates.

Fig. 6 displays the best-fitting RV curves and Table 5 lists the corresponding parameters. We note that we do not constrain the maximum RV separation, which is a source of uncertainty for the eccentricity and for the semi-amplitude of the RV curves. While we consider that the period is well constrained and that the system has likely a limited or no eccentricity, we regard other parameters as preliminary.

Under the adopted hypotheses, the component that we have referred to as the secondary appears to be the hotter, most massive component. Given the low amplitude of the RV curve, the minimum masses are very small, with values slightly below 1 M$_\odot$, suggesting an inclination of the order of 20°. This implies a deprojected rotational velocity for the fast rotating component of about 600 km s^{-1}. One possible channel to produce such a fast rotator is a recent mass transfer from the primary to the secondary that would have increased the secondary mass and spin it up to the critical rotation rate. If this scenario is correct, HD 101436 could turn out to be a very interesting system to constrain evolutionary scenarios of massive binaries. More data and, in particular a better coverage of the extrema of the RV curves, and the use of a disentangling algorithm to recover the line profiles independently of any assumption on their shapes are the needed ingredients to verify our preliminary analysis.

3.1.5 HD 101190

To the north of the cluster, HD 101190 (O6 V((f)); Walborn 1973) is reported as RV variable star (Ardeberg & Maurice 1977). Photometric monitoring by Balona (1992) also revealed significant variability
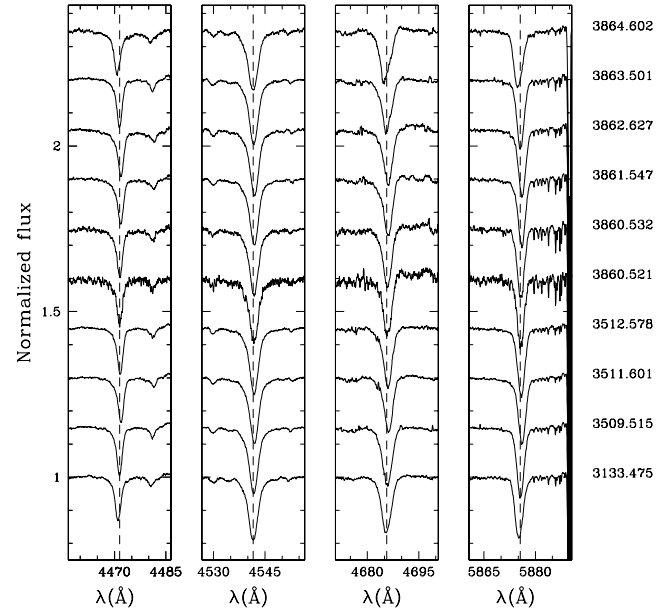
with an rms amplitude of 7 mmag although no period has been identified so far. We collected 20 spectra over a 4 yr timebase that shows relatively narrow lines, consistent with the rotational velocities deduced by Penny (1996) and Howarth et al. (1997) ($v \sin i = 89$ and 88 km s^{-1}, respectively). Our data further reveal clear variability of all the considered lines with asymmetric profiles seen at several epochs (see Fig. 7) . The He I lines show a larger RV amplitude than the He II lines but no secondary signature could be reliably disentangled by Gaussian fitting. Our classification criteria assign an O5.5 V((f)) spectral type to the composite spectra.

Inspection of the spectra reveals several interesting features. All the spectral lines in the HD 101190 spectrum display a clearly correlated motion, except the N III $\lambda\lambda$4634–4640 emission lines and the N V $\lambda\lambda$4604–4620 absorption lines that show constant velocity ($\sigma_{RV4604,4620} \approx 3$ km s^{-1}). On two occasions, the Si IV $\lambda\lambda$4089, 4116 lines are seen separated into a blueshifted absorption and a redshifted emission, the latter emissions displaying RVs consistent with those of the N III and N V lines. The presence of the N V $\lambda\lambda$4604–4620 absorptions and of the Si IV $\lambda\lambda$4089–4116 emissions is not compatible with the O6 V((f)) type reported by Walborn (1973), nor is it compatible with the average of the He I λ4471 over He II λ4542 ratio measured from our data. This suggests that the HD 101190 spectrum has two components: a very early O-type star that shows no RV variations and that is responsible of the N V absorptions and Si IV emissions, and a later O-type star which carries the RV signal.

Because we cannot detect the N IV λ4058 line and because the N V and Si IV lines are relatively faint, we assign the hotter star an O4 V((f+)) type, although we considered the O3.5 subtype within the uncertainties. Given the expected visible flux ratio between an O4 V star and a less massive O7 component ($\approx$2.75; Martins et al. 2005), one finds that an O7–O7.5 V star, with $W' \approx 1$, can reproduce the observed W' ratio of the composite spectrum. While our data do not allow us to prove that the O4 and O7 components are physically bound, we note that the chance alignment of two such stars is very small.
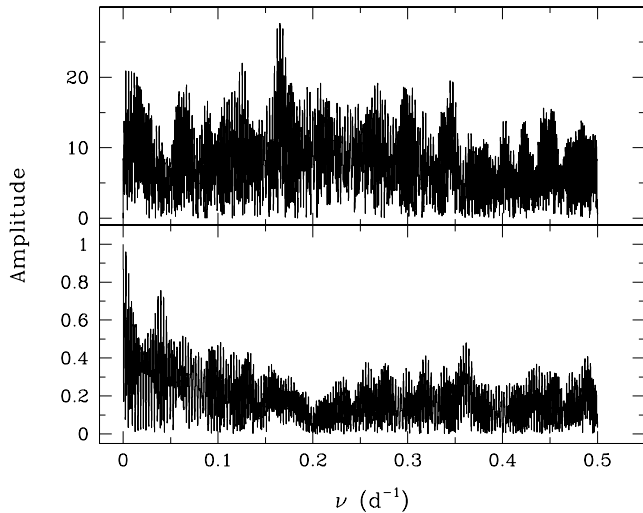
Figure 8. HD 101190: periodogram (upper panel) and spectral window (lower panel) computed using the average of the He I λλ4026, 4471, 4922, 5876 line RVs.

Table 6. HD 101190: best-fitting orbital solutions based on the He I and He II data sets. T (in HJD − 245 0000) is the time of periastron passage and is adopted as $\phi = 0.0$ in Fig. 9. Quoted uncertainties correspond to 1σ error bars.

Parameter	He I lines	He II lines
P (d)	6.0466 ± 0.0026	6.0473 ± 0.0026
e	0.29 ± 0.04	0.36 ± 0.07
ω (°)	117.8 ± 4.8	127.5 ± 6.2
T	2999.17 ± 0.09	2999.13 ± 0.11
γ_2 (km s^{-1})	-3.8 ± 0.7	8.2 ± 0.7
K_2 (km s^{-1})	34.4 ± 1.4	20.8 ± 1.2
rms (km s^{-1})	2.5	2.1

In an attempt to constrain the orbital properties of the system, we performed a Fourier analysis of the RV series associated with the individual He I and He II lines. All the data sets consistently yield an orbital period of 6.047 d, which is indeed the dominant alias in the periodogram (Fig. 8). We computed SB1 orbital solutions both using the RVs from the individual lines and by combining separately the He I λλ4026, 4471, 4922, 5876 and the He II λλ4200, 4542, 4686 RV measurements. Again we obtained very similar results. Table 6 and Fig. 9 give the best-fitting orbital solution for the He I and He II data sets and show the corresponding RV curves. While we consider that the orbital period is reliable, we note that the semi-amplitude of the RV curve K is likely a lower limit as it is affected by the blend with the O4 signature.

Finally, assuming that the secondary is not a very late O star, an hypothesis supported by the RV signatures in the He II lines, the binary mass ratio M_2/M_1 is likely larger than 0.3. This would imply a lower limit on the primary RV curve semi-amplitude: $K_1 > 10$ km s^{-1}, so that one would have expected to see some variations of the primary lines. While this argues against a direct bound between the O4 and the O7 star, we note that a mass ratio a factor of 2 lower than assumed here would solve this apparent discrepancy. Alternatively, the system may be triple, with a single hot star and an SB1 cooler star. More data are definitely needed to solve this issue.
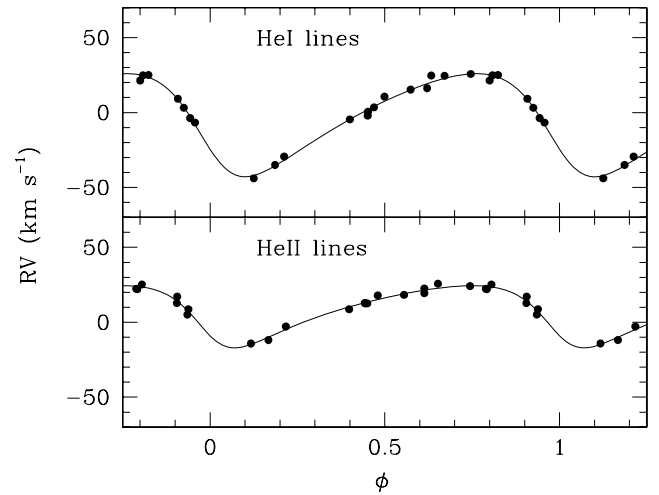

Figure 9. HD 101190: best-fitting RV curve for the He I (upper panel) and He II (lower panel) data sets.

3.1.6 HD 101413

HD 101413 (O8 V; Walborn 1973) is the visual companion of HD 101436, with a separation of 27.8 arcsec (Mason et al. 1998). Thackeray & Wesselink (1965) first reported large RV variations (ΔRV ∼ 100 km s^{-1}) based on three spectra collected over a year. *International Ultraviolet Explorer* (*IUE*) and *Far Ultraviolet Spectroscopic Explorer* (*FUSE*) rotational velocities were measured in the range 90–102 km s^{-1}(Penny 1996; Howarth et al. 1997; Penny & Gies 2009) and probably relate to the primary or to the composite spectrum. We obtained three FEROS spectra in 2005 May, two in 2006 May and a set of five UVES spectra spread over 3 months early 2008. The 2005 and some of the 2008 observations revealed the signature of the secondary component for the first time, although only in the He I lines (Fig. 10). A limited RV difference is seen on a day-to-day basis, but the primary and secondary smoothly varied
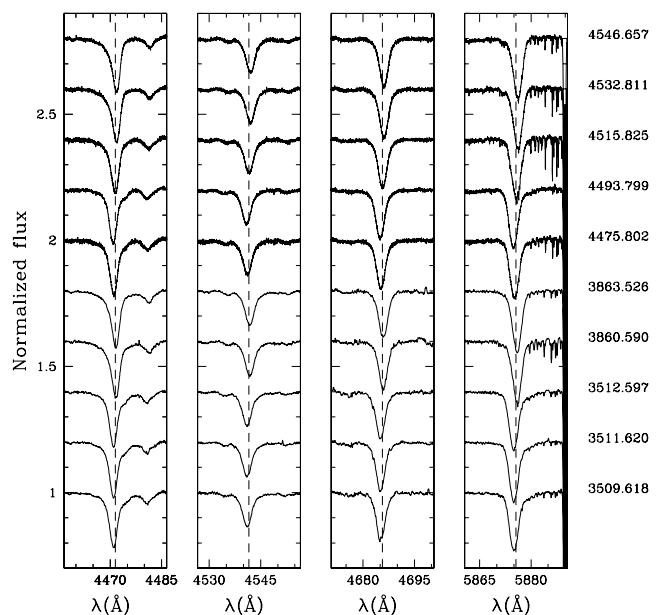

Figure 10. HD 101413: He I λ4471, He II λλ4542, 4686 and He I λ5876 line profiles at various epochs.

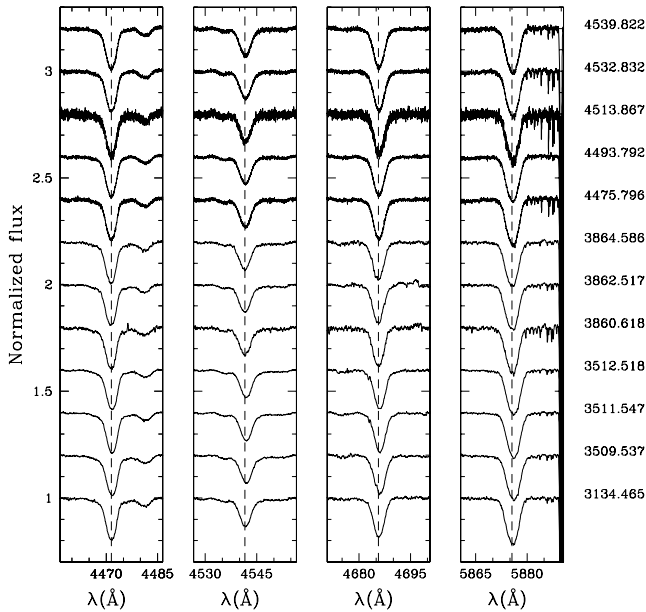**Figure 11.** HD 101191: He I λ4471, He II λλ4542, 4686 and He I λ5876 line profiles at various epochs.

Figure 12. HD 308813: He I λ4471, He II λλ4542, 4686 and He I λ5876 line profiles at various epochs.

from 2008 January to March, suggesting a period of 3 to 6 months. We note that we never observed such an extreme primary RV as the one reported by Thackeray & Wesselink (1965) in 1957 April ($RV_{prim} = -81\,km\,s^{-1}$). Using the few well-separated spectra, we confirm the primary O8 V classification. The companion spectrum shows neither He II nor Si IV lines and we assign it a B2-3 V classification. While we are missing a complete orbital coverage, empirical determination of the mass ratio can still be obtained. Based on the He I lines, we obtained $M_2/M_1 = 0.17 \pm 0.01$, which rather suggests a mid- to late-B type for the secondary.

3.2 SB1 systems

3.2.1 HD 101191

HD 101191 (O8 V((n)); Walborn 1973) is located at 1.4 arcmin south-west of HD 101205, in the core of the cluster and has been scarcely studied so far. We obtained 12 high-resolution spectra that reveal a clear SB1, long period signature (Fig. 11). Our different epochs indeed reveal RV variations with a peak-to-peak amplitude of $\approx 30\,km\,s^{-1}$ for the He II lines and of $\approx 20\,km\,s^{-1}$ for the He I lines. No significant night-to-night variability is observed, nor within the 3-month coverage of our UVES data. While we cannot rule out an alias at 20 d, such a period value is unlikely because the 3- and 5-d FEROS campaigns in 2005 May and 2006 May reveal no RV variation at all. This rather suggests a long orbital period, of several times the 3-month timebase of our UVES campaign. From our data, we can also place a relatively firm upper limit on the orbital period of about 4 yr. As the measured RVs display a relatively limited amplitude, we might have missed the epoch of maximum separation, keeping open the possibility that one can still observe the signatures of the two components. We derived an O8 V/III type for the composite spectrum. Because the He II λ4686 line is strongly seen in absorption, we adopt the O8 V spectral subtype as our final classification of the HD 101191 composite spectrum.
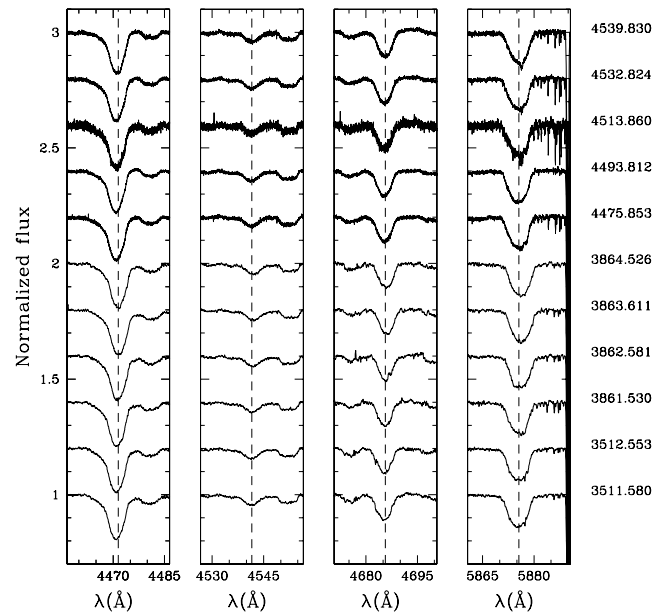
3.2.2 HD 308813

At 4.2 arcmin north-west of HD 101205, HD 308813 was classified O9.5 V by Schild (1970) and B0 V by Ardeberg & Maurice (1977). Thackeray & Wesselink (1965) observed it three times over a 2-yr time-scale and reported $\Delta RV \approx 28\,km\,s^{-1}$. Based on discrepant He II RVs compared to the He I ones, they proposed that HD 308813 is an SB2 candidate. Huang & Gies (2006a) also collected three observations over 4 d and reported RVs from 21.9 to $-17.6\,km\,s^{-1}$, confirming its SB1 nature. They further measured a projected rotational velocity $v\sin i$ of $196\,km\,s^{-1}$. We collected 11 spectra of HD 308813, covering time-scales from days to years. HD 308813 presents broad, somewhat variable lines (Fig. 12). We measured RVs using both Gaussian profile and purely rotationally broadened profiles and obtained very comparable results. Clear RV shifts (peak-to-peak difference over $40\,km\,s^{-1}$) are seen, although these are not happening as quickly as reported by Huang & Gies (2006a). All the lines follow the same orbital motion, so that we cannot confirm the SB2 nature of the object. We however note that some lines display systematic shifts in their RVs compared to the average. Given our data set, we cannot distinguish between a very short period system ($P < 2\,d$) and a longer one ($P > 20\,d$). With a clear He II λ4542 line, HD 308813 is not a B star but a late O star. We thus confirm the O9.5 V classification of Schild (1970).

3.3 Presumably single stars

3.3.1 HD 101298

The object was observed spectroscopically by Thackeray & Wesselink (1965), Conti et al. (1977) and Ardeberg & Maurice (1977). The latter reported possible RV variations within their four measurements. A 6-night photometric monitoring (Balona 1992), however, showed a constant luminosity. Similarly, no significant RV difference is observed in between the eight epochs of our campaign, which again suggests that the star is probably single (Fig. 13). Spectral type estimates point toward an O6–6.5 star. The W'' criterion is unsuited for such an early star as the He I λ4144 line has become
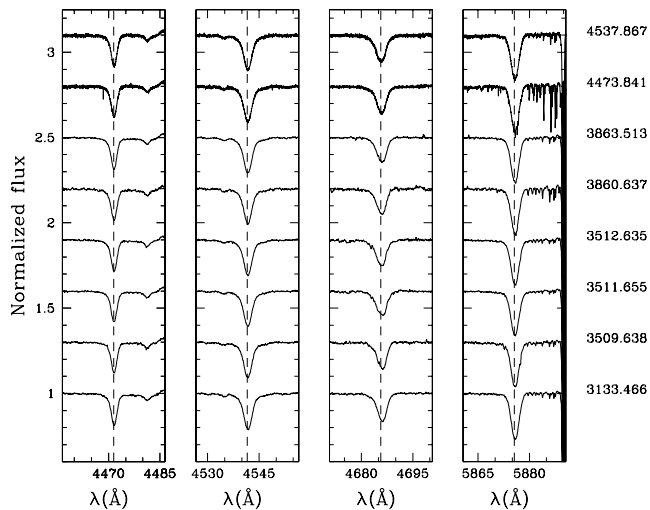
Figure 13. HD 101298: He I λ4471, He II λλ4542, 4686 and He I λ5876 line profiles at various epochs.

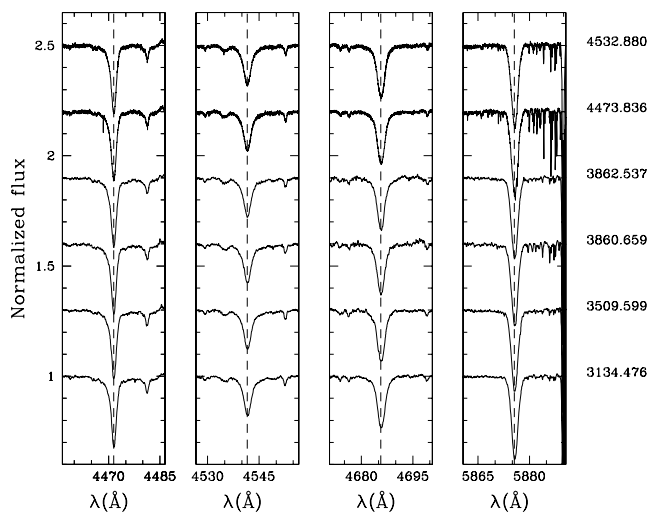**Figure 14.** HD 101223: He I λ4471, He II λλ4542, 4686 and He I λ5876 line profiles at various epochs.

very weak. With log $W(\lambda4686) \approx 2.7$, the He II λ4686 line suggests a giant classification. Being slightly variable while the other lines remain constant, the He II λ4686 line further suggests the presence of a significant wind, another hint of a slightly more evolved object. Following Walborn (1973), we adopt an O6 III((f)) classification. Note, however, that a class V would be in better agreement with the overall distance to the cluster (see Section 5.1).

3.3.2 HD 101223

Ardeberg & Maurice (1977) reported discrepant velocity measurements (ranging from -29 to $+4$ km s^{-1}) and asymmetrical line profile, suspecting HD 101223 to be a spectroscopic binary. Observed at six epochs over 5 yr (Fig. 14), the HD 101223 spectrum remains constant with a 1σ RV dispersion of the order of 1 km s^{-1}. The classification criteria indicate an O8 V/III star. Because the He II λ4686 line is strongly seen in absorption, we prefer the O8 V classification and we consider the star as single.
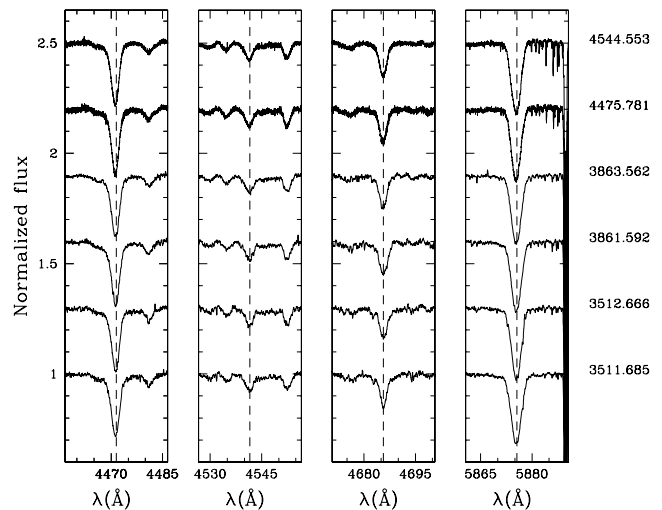

Figure 15. CPD $-62°2198$: He I λ4471, He II λλ4542, 4686 and He I λ5876 line profiles at various epochs.

3.3.3 CPD $-62°2198$

At about 30 arcmin north-west of the cluster centre, CPD $-62°2198$ presents a significantly different RV compared to other single stars (from about -6 to -12 km s^{-1} depending on the considered lines). Yet, we could not detect any significant RV variations within our six observations (Fig. 15) nor by comparison with older data by Reed & Kuhna (1997) and Huang & Gies (2006a). Classified as O9.5 Ib by Ardeberg & Maurice (1977), our He I λ4471 over He II λ4542 ratio indicates an O9.7 star, with the O9.5 subtype at 1σ. The $W(\lambda4089)/W(\lambda4144)$ ratio indicates a class III star while the log W''' criterion rather points to a class I star with class III within 1σ. Huang & Gies (2006b) obtained $T_{\rm eff} = 29132 \pm 375$ K and log $g = 3.556 \pm 0.039$ for CPD $-62°2198$, in good agreement with values expected for an O9.7 III star. We consider CPD $-62°2198$ to be likely single and we finally adopt the O9.7 III classification.

3.3.4 HD 101333

Classified B0 III, HD 101333 is a slow rotator ($v \sin i = 39$ km s^{-1}; Huang & Gies 2006a) in the southern part of the cluster. Thackeray & Wesselink (1965) and Huang & Gies (2006a) both reported a set of three RV measurements that show no internal discrepancy but these three sets differ by 15 km s^{-1} from each other. We obtained three FEROS spectra in 2006 May and another two UVES spectra in 2008 January and March. Several lines (e.g. He I λλ4144, 4388) display a clear Lorentz profile while others have a well-pronounced Gaussian shape. The UVES data are about 5 km s^{-1} larger than the FEROS measurements. Given the slow rotation, this is definitely significant although we cannot decide between a low-amplitude photospheric effect or a large mass ratio and/or low inclination binary scenario. The obtained spectral classification is somewhat dependent on the assumed line profile, but points to a late-type O star. Comparing HD 101333 with the spectral standards τ Sco (B0.2 V) and HD 98028 (O9 V) from Walborn & Fitzpatrick (1990) and to BD $-13°4930$ (O9.5 V) from Paper II (Fig. 16), we finally adopt an O9.5 V classification.

3.3.5 HD 101545A and B

HD 101545 is a visual binary the components of which are separated by a few arcsecs, the component A being to the north-east of
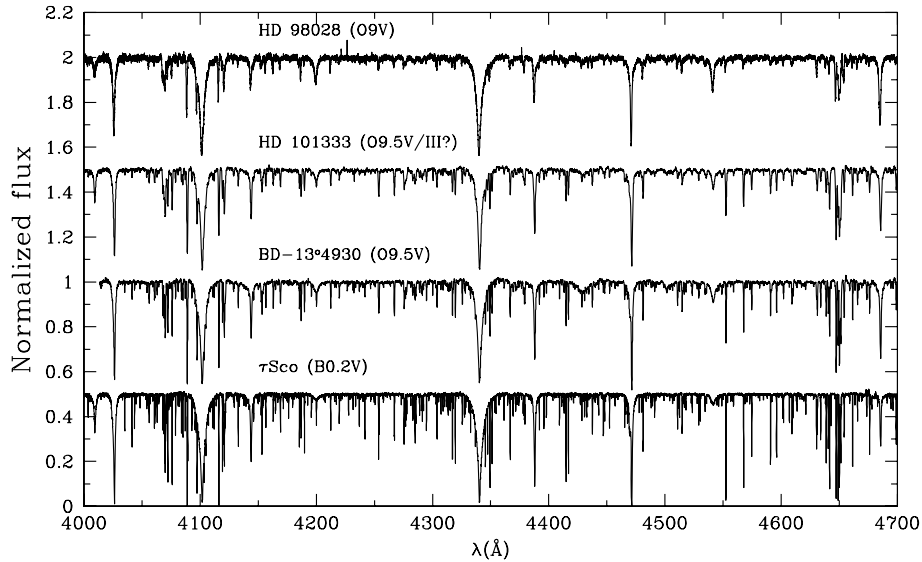
Figure 16. HD 101333: 4000–4700 Å spectral range compared to the spectroscopic standards τ Sco and HD 98028 and to BD $-13°4930$.
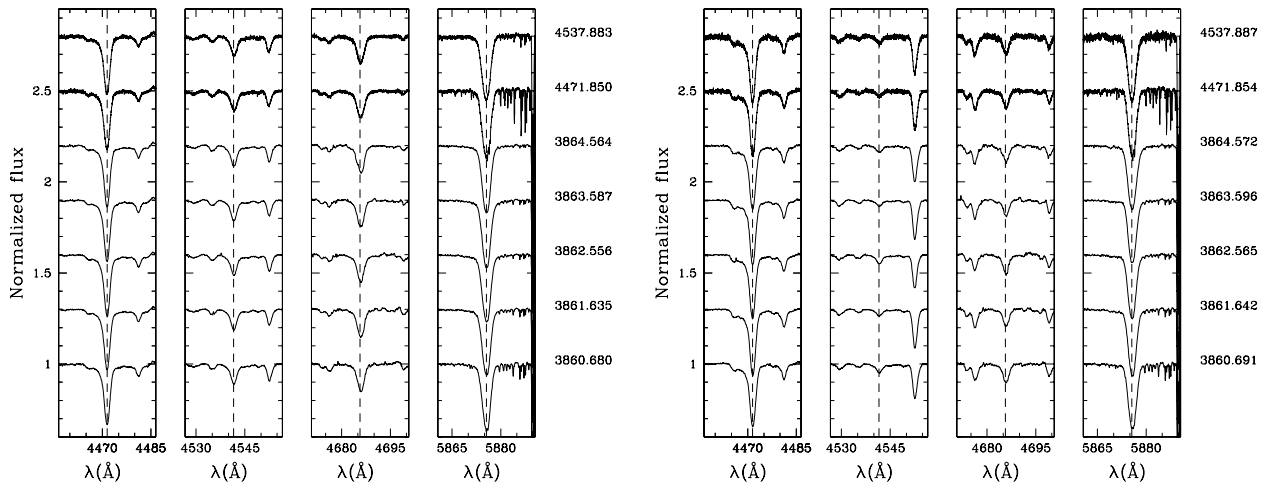

Figure 17. HD 101545A (left) and HD 101545B (right): He I $\lambda4471$, He II $\lambda\lambda4542$, 4686 and He I $\lambda5876$ line profiles at various epochs.

component B. Mason et al. (1998) reported a separation of 2.57 arcsec and respective V mag of 6.9 and 7.4. Both components are late O-type stars (Fig. 17). None of them displays any significant RV variation in their respective time series (seven spectra over 5 yr for each object of the pair). The best spectral type estimate yields O9.5 III/I and O9.7 III/I for the A and B components. Given the stars' brightness, we finally consider both stars to be giants and not supergiants.

3.4 Other stars in IC 2944

3.4.1 HD 308804

Reported as O9.5 V by Ardeberg & Maurice (1977), we observed HD 308804 twice with a 2 d separation. The HD 308804 spectrum contains neither He II nor Si IV lines and it is thus not the spectrum of an O star. While Ardeberg & Maurice (1977) mentioned double or asymmetric lines, our two spectra are single lined. Yet, they display a RV difference of $\sim$10 km s^{-1}, although the first spectrum has a much lower S/N compared to the second one. Huang & Gies (2006a) also observed this star three times over a four-night period

and reported no RV change. Their measured RV is however 10 and 20 km s^{-1} more negative than our two measurements, providing further support to the binary hypothesis. By comparison with the atlas of Walborn & Fitzpatrick (1990), we adopt a B3 V type for the composite spectrum of HD 308804.

4 OBSERVATIONAL BIASES

To estimate the impact of the observational biases on the detection probability of a binary with a given primary mass, we follow the approach described in Paper II. Briefly, we first draw a series of N SB2 systems adopting the following rules. The primary mass is fixed to the theoretical value of Martins et al. (2005) according to the primary spectral type of the considered object. The probability density function (PDF) of $\log P$(d) is taken to be uniform in the interval [0.3, 1.0] and [1.0, 3.5]. 50 per cent of the systems are spread in the first interval while the rest is distributed over the second interval. The eccentricity and mass ratio PDFs are taken to be uniform in the range [0.0, 0.9] and [0.1, 1.0], respectively, with the additional constraint that the separation at periastron is larger

Table 7. Binary detection probability for the time sampling associated with different objects (column 1) and for various period ranges (columns 2–5).

Time sampling	Short (2–10 d)	Intermediate (10–365 d)	Long (365–3000 d)	All (2–3000 d)
HD 100099	0.995	0.920	0.631	0.902
HD 101131	0.995	0.970	0.813	0.954
HD 101190	0.996	0.944	0.730	0.930
HD 101191	0.992	0.906	0.614	0.894
HD 101205	0.995	0.893	0.560	0.884
HD 101223	0.988	0.864	0.607	0.877
HD 101298	0.994	0.905	0.688	0.910
HD 101333	0.985	0.759	0.324	0.789
HD 101413	0.992	0.900	0.530	0.876
HD 101436	0.995	0.915	0.568	0.891
HD 101545A	0.991	0.783	0.376	0.810
HD 101545B	0.992	0.785	0.341	0.805
HD 308813	0.992	0.886	0.463	0.859
CPD −62°2198	0.987	0.839	0.511	0.851

than $20\,R_\odot$ to avoid contact. Finally, the orbital configuration of each system is drawn assuming a random orientation in space and a random time of periastron passage.

We then applied the time sampling corresponding to the observations of a given object to the RV curve of each of the N SB2 binaries and we computed what would have been the largest RV difference (ΔRV) recorded. The detection probability P_{detect} is then given by the ratio of the systems that display ΔRV larger than a given threshold C:

$$P_{\text{detect}} = \frac{N(\Delta\text{RV} > C)}{N}. \tag{1}$$

In the results presented in Table 7, we adopted $C = 20\,\text{km\,s}^{-1}$ and we computed P_{detect} for various ranges of the orbital periods. Our overall detection probability is better than 0.8 for all the objects, with the main uncertainties coming from the long period range. Based on those results one can exclude that the objects reported as single (Section 3.3) are short-period binaries ($P < 10\,\text{d}$). Some of them could still be undetected long-period binaries. Yet, given that such systems are expected to be rare (Sana & Evans 2010), the chance of having at least one undetected system among the six presumably single objects is 0.56.

Fig. 18 displays the probability density function of detecting a given number of binaries assuming all the objects in IC 2944 are multiple systems. It reveals that the probability to detect eight binaries or less is 0.002, allowing thus to reject the null hypothesis of $f_{\text{true}} = 1.0$. This plot also indicates that the most likely binary detection rate of our campaign is close to 0.9.

As discussed in Paper II, our simulations neglect the effect of line blending, that decreases the detection probability of near equal flux systems and/or of systems with large projected rotational velocities. Among our sample, HD 308813 displays the broadest lines ($v\sin i \sim 200\,\text{km\,s}^{-1}$), yet RV variations with a peak-to-peak amplitude of $\sim 40\,\text{km\,s}^{-1}$ are clearly detected. All the presumably single stars discussed in Section 3.3 have significantly narrower line profiles so that even small RV variations in an equal-flux system would induce significant changes in these line profiles. Finally, we note that the main limitations of our simulations lay in the adopted distributions of orbital parameters. While our assumptions are in line with earlier results from our campaign as well as with the preliminary results of Sana & Evans (2010), it is unknown whether the multiplicity properties of O stars are homogeneous or show sizeable variations from one cluster to another.
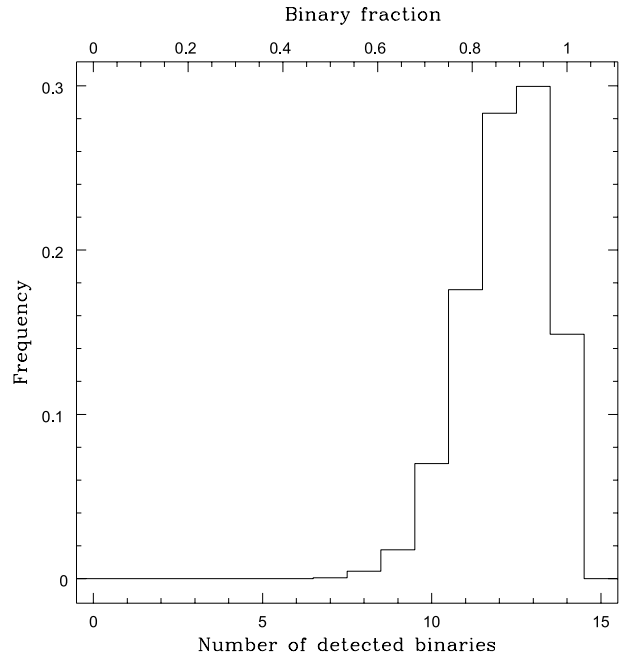
Figure 18. Distribution of the number of detected SB systems as obtained from 10 000 realizations of a cluster with 14 O-type binaries.

5 DISCUSSION

5.1 Distance and membership

As already discussed in the Introduction, several authors questioned the single nature of the IC 2944 complex and preferred to rather consider several OB associations along the line of sight. Using our refined spectral classifications, we recompute the distance modulus (DM) of each target in our sample using both the V- and K-band magnitudes (Table 8). In this exercise, we adopted the theoretical absolute magnitudes, colours and bolometric corrections from Martins & Plez (2006) and the interstellar extinction law of Fitzpatrick (1999).

The revision of the spectral classification and more particularly of the multiplicity status of the components leads to significant changes in the spectroscopic parallax of the objects. The most critical examples are probably the cases of HD 101191 and HD 101545 which are now located at a distance compatible with the other objects in IC 2944. The largest deviations are shown by HD 308804 and CPD −62°2198 and these stars might, respectively, be foreground and background objects. HD 101298 also seems slightly more distant. As noted earlier, adopting a main-sequence classification instead of a giant one would bring the star in perfect agreement with the cluster mean distance. Ignoring these three stars as well as HD 101205 due to its uncertain number of components, the estimated distance to IC 2944 is 2.3 ± 0.3 kpc, in perfect agreement with the earlier estimates of Thackeray & Wesselink (1965) and Tovmassian et al. (1998), but relatively larger than the 1.8 kpc estimate of Kharchenko et al. (2005). More interestingly, we cannot identify significant differences between the various subgroups of stars in IC 2944, suggesting that most of the O stars belong to a single entity.

Finally, the dynamical properties of the objects compared to the average properties of the sample can also be used as a membership criterion. From Fig. 19, and beside the binaries, only
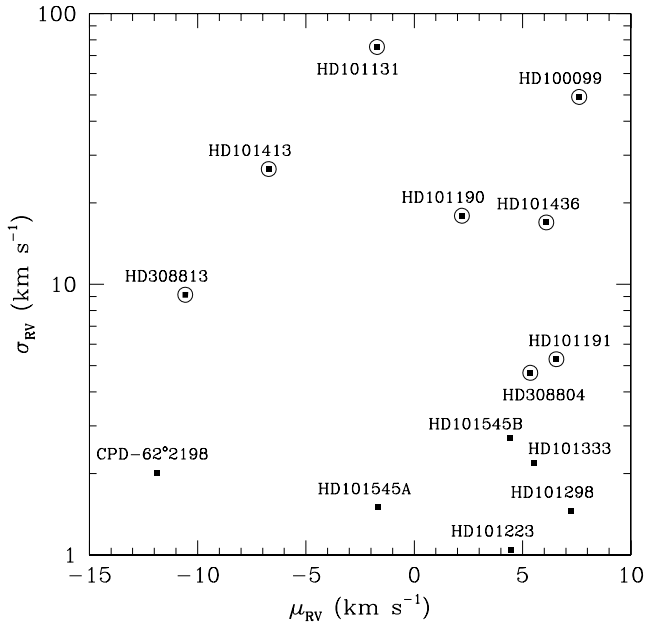
Figure 19. Dispersion of the He I λ5876 RV measurements versus their mean RV. Circles around the $\sigma-\mu$ points indicate the binaries. The average systemic velocities have been used instead of the mean RV for the binaries with orbital solutions: HD 100099, HD 101131, HD 101190 and HD 101436.

Table 8. Colour excess and spectroscopic DM computed from the *V* and *K* band magnitudes.

Object	$E(B-V)$	DM_V	DM_K
HD 100099	0.36	12.57 ± 0.26	12.31 ± 0.07
HD 101131	0.27	11.68 ± 0.40	11.40 ± 0.11
HD 101190	0.37	12.08 ± 0.50	12.12 ± 0.21
HD 101205	0.30	11.43 ± 0.73	11.08 ± 0.10
HD 101413	0.30	11.86 ± 0.28	11.58 ± 0.13
HD 101436	0.32	12.14 ± 0.50	12.00 ± 0.11
HD 101191	0.28	12.03 ± 0.14	11.79 ± 0.14
HD 308804	0.40	11.73 ± 0.55	10.82 ± 0.05
HD 308813	0.29	12.28 ± 0.16	12.17 ± 0.09
HD 101223	0.43	11.77 ± 0.15	11.63 ± 0.14
HD 101298	0.31	12.86 ± 0.09	12.57 ± 0.08
HD 101333	0.31	12.02 ± 0.16	11.75 ± 0.09
HD 101545AB	0.23	12.16 ± 0.32	11.40 ± 0.05
CPD −62°2198	0.39	14.46 ± 0.07	13.05 ± 0.05

CPD −62°2198 displays a significant RV difference compared to the systemic velocity of the cluster. Combined with the significantly different reddening and distance for the object (Table 8), CPD −62°2198 potentially is a much more distant star seen along the line of sight to IC 2944.

5.2 Binary fraction

Eight objects out of 14 O-type stars shows a clear SB signature, yielding a minimal binary fraction of $f_{min} = 0.57$. Statistical uncertainties due to the limited size of our sample amounts to ± 0.13 (1σ error bar). Using the results of Section 4, the observed binary fraction likely corresponds to a true binary fraction $f_{true} = 0.65$. Proportionally, this makes this sample one of the richest binary nest after NGC 6231 (Sana et al. 2008, hereafter Paper I). Yet, some ob-

jects might not belong to IC 2944 itself. For example, HD 100099 and HD 101545AB are significantly offset from the cluster core and CPD −62°2198 seems much more distant than IC 2944. Rejecting these three objects, the SB fraction in IC 2944 would increase to 0.70.

Beside HD 101205, HD 101413 and HD 101545, Mason et al. (1998) note single star results from speckle observations of six targets in Table 9: HD 100099, HD 101131, HD 101123, HD 101298, HD 101413 and HD 101436. Within a radius of 3 arcsec, the average number of companion per primary O star is thus of 0.84 and is again very similar to the value obtained in NGC 6231. As in the previous papers of this series, close to 70 per cent of the O star population is to be found in spectroscopic binary systems.

5.3 Orbital parameters

Among the eight spectroscopic binaries in our sample, three have periods up to 10 d, two others have periods of several tens of days and the last three systems are longer period binaries with, most likely, an orbital time-scale of the order of months to years. While the sample is likely too small to significantly constrain the overall period distribution, we note that there is no obvious contradiction with the period distribution derived for the binaries in NGC 6231 (Paper I), neither with the preliminary results of Sana & Evans (2010). Similarly, the mass ratio distribution is poorly sampled but would qualitatively follow the uniform distribution suggested by Sana & Evans (2010).

6 SUMMARY

Based on a set of 171 high-resolution high S/N optical spectra, we revisited the status of 14 early-type objects in IC 2944 and the Cen OB2 association. We presented new evidence of binarity for five objects and we confirmed the multiple nature of another two. We derived the first orbital solutions for HD 100099, HD 101436 and HD 101190 and provide additional support for a higher multiplicity in HD 101205. The minimal spectroscopic binary fraction in our sample is 0.57 but rises to 0.63 if one only considers the objects located in the inner 12 arcmin around HD 101205. Our sample is limited and does not provide strong constraints on the distribution of the orbital parameters of the binary systems. Yet, no sizeable disagreement is observed with results from earlier papers in this series, nor with the preliminary results of Sana & Evans (2010) that combine data from several clusters. Using an approach similar to the one presented in Paper II, we estimated the observational biases of our campaign and we showed that the binary detection rate is close to 90 per cent, leaving thus little room for undetected systems. Using newly derived spectroscopic parallaxes, we reassessed the distance to IC 2944. We confirm that, as far as the O stars are concerned, the cluster is most likely a single entity and that HD 101545 and HD 100099, offset by 50–60 arcmin from the cluster core, are located at a similar distance as IC 2944.

Table 9. Final spectroscopic classification and multiplicity properties of the studied O stars in IC 2944. An 'O' appended to the SB1/2 flag means that an orbital solution is available; an 'E', that the system displays eclipses in addition to its SB signature.

Object	Mult.	Spectral type		M_2/M_1	P	e
		Previous works	This work		(d)	
SB2 systems						
HD 100099	SB2O	O9 III	O9III+O9.7 V	0.792	21.56	0.52
HD 101131	SB2O	O6.5 V((f))+O8.5 V	n/a	0.56	9.65	0.16
HD 101190	SB2O	O5.5–O6 V((f))	O4 V((f))+O7 V	0.3–0.5	6.05	≈0.3
HD 101205	SB2OE	O7 IIIn((f))	n/a	undef.	2.1–2.8	0.0
HD 101413	SB2	O8 V	O8 V+B3: V	≈0.2	1–2×10^2	undef.
HD 101436	SB2	O6.5 V	O6.5 V+O7V	0.52–0.79^a	37.37	0.11
SB1 systems						
HD 101191	SB1	O8 V((n))	O8 V	undef.	10^2–10^3	undef.
HD 308804	SB1	O9.5 V	B3 V	undef.	>5	undef.
HD 308813	SB1	O9.5 V–B0 V	O9.5 V	undef.	undef.	undef.
Single stars						
HD 101223	sgl.	O8 V((f))	O8 V	n/a	n/a	n/a
HD 101298	sgl.	O6 III((f))	O6 III((f))	n/a	n/a	n/a
HD 101333	sgl.	O9.5–B0 III	O9.5 V	n/a	n/a	n/a
HD 101545A	sgl.	O9.5–B0.5 Ib	O9.5 III	n/a	n/a	n/a
HD 101545B	sgl.	O9.5–B0.5 Ib	O9.7 III	n/a	n/a	n/a
CPD −62°2198	sgl.	O9.5 Ib	O9.7 III	n/a	n/a	n/a

^{a}For comparison purpose, we have inverted the primary and secondary identification so that the mass ratio is smaller than unity in the present table.

REFERENCES

Alter G., Balazs B., Ruprecht J., Vanysek J., 1970, Catalogue of Star Clusters and Associations. Akademiai Kiado, Budapest
Ardeberg A., Maurice E., 1977, A&AS, 28, 153
Ardeberg A., Maurice E., 1980, A&AS, 39, 325
Balona L. A., 1992, MNRAS, 254, 404
Baumgardt H., Dettbarn C., Wielen R., 2000, A&AS, 146, 251
Charbonneau P., 1995, ApJS, 101, 309
Collinder P., 1931, Ann. Obser. Lund, 2, 1
Conti P. S., 1973, ApJ, 179, 181
Conti P. S., Alschuler W. R., 1971, ApJ, 170, 325
Conti P. S., Leep E. M., Lorre J. J., 1977, ApJ, 214, 759
Fitzpatrick E. L., 1999, PASP, 111, 63
François P. et al., 2007, A&A, 476, 935
Garrison R. F., Hiltner W. A., Schild R. E., 1977, ApJS, 35, 111
Gies D. R., Penny L. R., Mayer P., Drechsel H., Lorenz R., 2002, ApJ, 574, 957
Gosset E., Royer P., Rauw G., Manfroid J., Vreux J.-M., 2001, MNRAS, 327, 435
Heck A., Manfroid J., Mersch G., 1985, A&AS, 59, 63
Herbst W., 1975, AJ, 80, 212
Howarth I. D., Siebert K. W., Hussain G. A. J., Prinja R. K., 1997, MNRAS, 284, 265
Huang W., Gies D. R., 2006a, ApJ, 648, 580
Huang W., Gies D. R., 2006b, ApJ, 648, 591
Humphreys R. M., 1973, A&AS, 9, 85
James G., François P., Bonifacio P., Carretta E., Gratton R. G., Spite F., 2004, A&A, 427, 825

Kharchenko N. V., Piskunov A. E., Röser S., Schilbach E., Scholz R.-D., 2005, A&A, 438, 1163
Martins F., Plez B., 2006, A&A, 457, 637
Martins F., Schaerer D., Hillier D. J., 2005, A&A, 436, 1049
Mason B. D., Gies D. R., Hartkopf W. I., Bagnuolo W. G., ten Brummelaar T., McAlister H. A., 1998, AJ, 115, 821
Mathys G., 1988, A&AS, 76, 427
Mathys G., 1989, A&AS, 81, 237
Mayer P., Lorenz R., Drechsel H., 1992, Inf. Bull. Var. Stars, 3765, 1
Mayer P., Božić H., Lorenz R., Drechsel H., 2010, Astron. Nachrichten, 331, 274
Mermilliod J.-C., 1992, Bull. Inf. CDS, 40, 115
Otero S. A., 2007, Open European J. Var. Stars, 72, 1
Penny L. R., 1996, ApJ, 463, 737
Penny L. R., Gies D. R., 2009, ApJ, 700, 844
Perry C. L., Landolt A. U., 1986, AJ, 92, 844
Puls J., Urbaneja M. A., Venero R., Repolust T., Springmann U., Jokuthy A., Mokiem M. R., 2005, A&A, 435, 669
Reed B. C., Kuhna K. M., 1997, AJ, 113, 823
Reipurth B., Corporon P., Olberg M., Tenorio-Tagle G., 1997, A&A, 327, 1185
Reipurth B., Raga A., Heathcote S., 2003, AJ, 126, 1925
Sana H., Evans C., 2010, in Neiner C., Wade G., Meynet G., Peters G., eds, Proc. IAU Symp. 272, Active OB Stars. Cambridge Univ. Press, Cambridge, in press (arXiv:1009.41975)
Sana H., Rauw G., Gosset E., 2001, A&A, 370, 121
Sana H., Gosset E., Rauw G., 2006, MNRAS, 371, 67
Sana H., Gosset E., Nazé Y., Rauw G., Linder N., 2008, MNRAS, 386, 447 (Paper I)
Sana H., Gosset E., Evans C. J., 2009, MNRAS, 400, 1479 (Paper II)
Schild R. E., 1970, ApJ, 161, 855
Thackeray A. D., 1950, MNRAS, 110, 524
Thackeray A. D., Wesselink A. J., 1965, MNRAS, 131, 121
Tovmassian H. M. et al., 1988, Pis'ma Astron. Zh., 14, 291

Tovmassian H. M., Epremian R. A., Hovhannessian K., Cruz-Gonzalez G., Navarro S. G., Karapetian A. A., 1998, AJ, 115, 1083
Vega E. I., Orsatti A. M., Marraco H. G., 1994, AJ, 108, 1834
Walborn N. R., 1973, AJ, 78, 1067
Walborn N. R., 1987, AJ, 93, 868
Walborn N. R., Fitzpatrick E. L., 1990, PASP, 102, 379

SUPPORTING INFORMATION

Additional Supporting Information may be found in the online version of this article:

Table 2. Journal of the spectroscopic observations of the O-type stars in IC 2944.

Please note: Wiley-Blackwell are not responsible for the content or functionality of any supporting materials supplied by the authors. Any queries (other than missing material) should be directed to the corresponding author for the article.

This paper has been typeset from a TEX/LATEX file prepared by the author.